

# Supporting Information

## Chemical Vapor Deposited Polymer Layer for Efficient Passivation of Planar Perovskite Solar Cells

Mahdi Malekshahi Byranvand,<sup>a,b†</sup> Farid Behboodi-Sadabad,<sup>c†\*</sup> Abed Alrhman Eliwi,<sup>b</sup> Vanessa Trouillet,<sup>d,e</sup> Alexander Welle,<sup>c,e</sup> Simon Ternes,<sup>a,b</sup> Ihteaz Muhaimen Hossain,<sup>a,b</sup> Motiur Rahman Khan,<sup>b</sup> Jonas Alexander Schwenzer,<sup>b</sup> Amjad Farooq,<sup>a,b</sup> Bryce Sydney Richards,<sup>a,b</sup> Joerg Lahann<sup>c,f\*</sup> and Ulrich Wilhelm Paetzold<sup>a,b\*</sup>

<sup>a</sup> Institute of Microstructure Technology, Karlsruhe Institute of Technology, Hermann-von-Helmholtz-Platz 1, 76344 Eggenstein-Leopoldshafen, Germany.

E-mail: ulrich.paetzold@kit.edu

<sup>b</sup> Light Technology Institute, Karlsruhe Institute of Technology, Engesserstrasse 13, 76131 Karlsruhe, Germany.

<sup>c</sup> Institute of Functional Interfaces, Karlsruhe Institute of Technology, Hermann-von-Helmholtz-Platz 1, 76344 Eggenstein-Leopoldshafen, Germany.

E-mail: farid.sadabad@kit.edu, joerg.lahann@kit.edu

<sup>d</sup> Institute for Applied Materials, Karlsruhe Institute of Technology, 76344 Eggenstein-Leopoldshafen, Germany.

<sup>e</sup> Karlsruhe Nano Micro Facility, Karlsruhe Institute of Technology, 76344 Eggenstein-Leopoldshafen, Germany.

<sup>f</sup> Biointerfaces Institute and Departments of Chemical Engineering, Materials Science and Engineering, Macromolecular Science and Engineering and Biomedical Engineering, University of Michigan, Ann Arbor, Michigan 48109, USA.

† These authors contributed equally to this work.

**Content:**

**Experimental section** .....6

**Supplementary Figures and Tables**.....14

**Scheme S1.** Simplified schematic of the deposition chamber of the CVD set up with dimensions.....14

**Figure S1.** Deposition characteristic of PPX: thickness of the PPX layer as a function of the amount of the monomer fed into the CVD setup. A precise amount of the monomer was placed into a container from a stock solution of the monomer (20 mg/mL [2.2]paracyclophane in acetone). After evaporation of the solvent (<1 min), the container with monomer was transferred into the sublimation zone of the CVD and used to coat silicon wafers placed on the sample holder. The thickness values (nm) of PPX layer on the silicon wafer were obtained by ellipsometry.....15

**Figure S2.** Deposition of a uniform and continuous film of PPX with controlled thickness: SEM images of the cross section of the silicon wafer coated with PPX layer with thicknesses of (a) 50 nm, (b) 25 nm, and (c) 10 nm.....15

**Figure S3.** Relative intensity of depth integrated  $C_3H_8^+$  signals (characteristic for PPX polymer deposited on the surface of the perovskite) obtained from ToF-SIMS depth profiling of uncoated perovskite and perovskite coated with 0.5 nm, 1 nm, 2 nm, and 5 nm PPX.....16

**Figure S4.** (a) Detailed XPS C 1s spectra of a silicon wafer placed on the sample holder of the CVD setup with switched off oven (no pyrolysis) (bottom) and of a silicon wafer coated with a 10 nm PPX layer obtained under normal CVD condition (oven switched on) after washing with ethanol and acetone (top). Only for the PPX layer, the weak  $\pi-\pi^*$  transition signal at  $\sim 291.5$  eV is

appearing. For a better visualization, all spectra are normalized to the maximum of intensity. (b) The C8H8 fragment, although being present in the individual building blocks as well, is only detectable if the pyrolysis oven is used to create reactive species being able to form polymer (shown in gray color). Without pyrolysis no similar signal can be observed (shown in green and red color for sample before and after washing respectively).....17

**Figure S5.** Top view SEM images of (a) uncoated, (b) 1 nm PPX-coated, and (c) 5 nm PPX-coated perovskite thin films. (d) XRD patterns and (e) normalized absorbance spectra the same samples. ....18

**Figure S6.** Cross-sectional SEM images of full PSCs fabricated by (a) uncoated and (b) 1 nm PPX-coated perovskite thin films.....18

**Figure S7.** (a) Champion revers (R, solid line) and forward (F, dash line) J–V characteristics (b) stabilized PCEs during MPP tracking of PSCs fabricated with various thicknesses of the PPX passivation layer.....19

**Figure S8.** Histograms of the photovoltaic parameters in both revers and forward *J-V* direction for 25 PSCs.....20

**Scheme S2.** Scheme showing the dimensions of the sample holder that enables to deposit PPX layer on a relatively large area of 15 cm in diameter. Up to 16 samples can be loaded on the sample holder in one run.....21

**Figure S9.** Measured data (Psi, Delta) from ellipsometry experiments (solid lines) of PPX layers of nominal thickness around 1 nm and the constructed model to describe the experimental data (dashed lines) using either (a,b) silicon wafer as the substrate or (c,d) perovskite as the substrate. (e) Optical constant refractive index (*n*) of PPX layer (Cauchy model for transparent material assumes an extinction coefficient  $k = 0$ ) as a function of wavelength. Given that PPX exhibits some

absorption for wavelength  $< 370$  nm, the refractive index is shown only for a limited spectral range (370 nm-900 nm). A mean squared error (MSE) of 1.302 (for silicon wafer sample) and 6.444 (for perovskite sample) with a thickness of  $1.02 \pm 0.072$  nm and  $1.05 \pm 0.141$  nm was obtained as a result of the fit for the PPX layer deposited on (a,b) the silicon wafer and (c,d) perovskite, respectively.

.....22

**Figure S10.** (a) Reverse (R) and forward (F)  $J-V$  characteristics of four champion solar cells with 1 nm PPX-coated perovskite thin film (inset: photo of the device). (b) Power conversion efficiency ( $PCE$ ) in both direction of 25 PSCs for different runs of CVD passivation.....23

**Figure S11.** External quantum efficiency (EQE) spectra of PSCs incorporating an uncoated (black) and a 1 nm PPX-coated (red) perovskite thin film. ....23

**Figure S12.** Delta ( $\Delta$ ) of photovoltaic parameters extracted from the  $J-V$  measurement of different thicknesses of PPX passivation layers (a-c) and different concentration of PMMA solution that are used to spin coat the PMMA passivation (e-h).....24

**Figure S13.** The normalized MPP tracking of the PSCs under continuous illumination for 60 min. ....25

**Figure S14.** Photovoltaic parameters extracted from  $J-V$  characteristics of 10 reference PSCs that were not exposed to a CVD process conditions (“No CVD”) and 10 PSCs that underwent the entire CVD deposition process but without any precursor being supplied during the deposition step: (a)  $V_{OC}$ , (b)  $FF$ , (c)  $J_{SC}$  and (d)  $PCE$ .....25

**Figure S15.**  $V_{OC}$  vs. light intensity measurements derived from PSCs incorporating an uncoated (black) and 1 nm PPX-coated (red) perovskite thin films. ....26

**Figure S16.** Water contact angles (CA) measured on various perovskite thin films: (a) uncoated, (b) 1 nm PPX-coated and (c) 5 nm PPX-coated perovskite thin films. ....26

**Figure S17.** AFM images obtained at several time points from (a) uncoated, (b) 1 nm PPX-coated and (c) 5 nm PPX-coated perovskite thin films for 24 h under ambient air conditions. ....27

**Figure S18.** Surface roughness of marked perovskite grains for uncoated, 1 nm PPX-coated and 5 nm PPX-coated perovskite thin films before and after 24 h under ambient air conditions.....28

**Figure S19.** Photographs of PSCs fabricated by uncoated, 1 nm and 5 nm PPX-coated perovskite thin films at the beginning and after 30 days stability test. ....28

**Figure S20.** (a-c) XRD pattern of perovskite thin films without and with 1 nm and 5 nm PPX passivation layer. The XRD pattern of the films are compared before and after a humidity stress test (75% humidity, dark, 25 °C). (d) The PCEs and photographs (inset) of PSCs processed from perovskite thin films stressed as discussed in (a-c).....29

**Table S1.** Thicknesses of PPX layers determined by ellipsometry measurements, for several spots on three random substrates per PPX deposition (targeted thickness of 0.5 nm, 1 nm, 2 nm and 5 nm).....30

**Table S2.** Reverse (R) and forward (F) photovoltaic parameters of champion PSCs with various thicknesses of PPX layer.....31

**Table S3.** Reverse (R) and forward (F) photovoltaic parameters obtained for four solar cells of the champion PSC fabricated by 1 nm PPX-coated perovskite thin film.....32

**Table S4.** Photovoltaic parameters obtained from the champion PSCs – under reverse (R) and forward (F) scans – fabricated by uncoated and 1 nm PPX-coated perovskite thin films.....32

**References**.....33

## **Experimental Section**

***Perovskite solar cells Fabrication:*** The Perovskite solar cells (PSCs) were fabricated in in n-i-p solar cell architecture: glass substrate, indium tin oxide (ITO)/nanoparticle-based SnO<sub>2</sub> electron transport layer (ETL)/double-cation perovskite absorber layer/2,2',7,7'-tetrakis(N, N'-di-p-methoxy phenylamine)-9,9'-spirobifluorene (SpiroOMeTAD) hole transport layer (HTL)/gold back electrode.

The prepatterned ITO-on-glass substrates (sheet resistance 15 Ω sq<sup>-1</sup>, Luminescence Technology) were cleaned consecutively with deionized (DI) water, acetone, and isopropyl alcohol (IPA, Sigma-Aldrich) in an ultrasonic bath for 10 min, followed by oxygen plasma cleaning at 100 W power for 3 min. In the next step, a thin layer of nanoparticle-based SnO<sub>2</sub> ETL was spin coated on ITO substrates (4000 rpm for 30 s), followed by an annealing step at 250 °C for 30 min. The 2.04 wt% SnO<sub>2</sub> colloids solution was prepared by the diluting colloidal dispersion of SnO<sub>2</sub> nanoparticles (Alfa Aesar, 15 wt% aqueous solution) in DI water.

The perovskite absorber ((FAPbI<sub>3</sub>)<sub>0.97</sub>(MAPbBr<sub>3</sub>)<sub>0.03</sub>) thin films were deposited on top of the SnO<sub>2</sub> ETL substrate via a two-step spin coating process. It should be noted that before depositing the perovskite thin film, the ETL substrates were treated with oxygen plasma cleaning at 30 W power for 1 min to improve the surface wetting. First, lead iodide (PbI<sub>2</sub>) solution was spin coated at 1500 rpm for 30 s and annealed at 70 °C for 1 min. The PbI<sub>2</sub> precursor solution (1.3 M) was prepared by dissolving PbI<sub>2</sub> (Sigma-Aldrich, 99.999%) in the 9.5:0.5 (volume ratio) solvent mixture of N,N-dimethylformamide (DMF, Sigma Aldrich, anhydrous, 99.8%) and dimethyl sulfoxide (DMSO, Sigma Aldrich, anhydrous, ≥99.9%). Second, a solution of 60 mg formamidinium iodide (FAI,

GreatCell Solar), 6 mg methylammonium bromide (MABr, GreatCell Solar) and 6 mg methylammonium chloride (MACl, Lumtec) in 1 ml isopropyl alcohol (IPA) were spin-coated onto the  $\text{PbI}_2$  thin films at a spin rate of 1300 rpm for 30 s, followed by a thermal annealing step at 150 °C for 15 min in ambient conditions (30–40% humidity). Afterward, the perovskite thin films were transferred into a  $\text{N}_2$ -filled glovebox for the subsequent processing steps.

The poly(*p*-xylylene) (PPX) ultra-thin films were deposited by chemical vapor deposition (CVD) polymerization method using the custom-built setup described elsewhere.<sup>1</sup> In this CVD process, the [2.2]paracyclophane (Curtiss-Wright Surface Technologies (Galway, Ireland)) monomer sublimates at elevated temperatures (90-120 °C) and under reduced pressure (0.12 mbar) and later forms free radicals during the pyrolysis step at 660 °C, while flowing through a 320 mm long quartz tube with the carrier gas (Ar, flow rate 20 sccm). Finally, the polymerization occurs on top of the cooled (~14-16 °C) rotating (30 rpm) substrate in the deposition chamber that is equipped with a rotatable cooled sample holder. Therefore, the substrates on the sample holder are not exposed to high temperatures at all.

The thickness of the deposited PPX layer was controlled in each experiment by feeding a precise amount of monomer into the setup. A precise amount of the monomer was placed into the sublimation zone of the CVD. To obtain a PPX layer with the nominal thickness value of 0.2 nm, 0.5 nm, 1 nm, 2 nm, 5 nm the CVD was performed for 5 min with the corresponding amount of monomer of 1.0 mg, 1.6 mg, 2.4 mg, 4.7 mg, and 10.8 mg fed into the sublimation zone, respectively (see Fig. S1 for the whole range). The film thickness was monitored after the deposition with a multi wavelength rotating analyzer ellipsometer (M-44, J. A. Woollam) on both the perovskite films and a control silicon wafer.<sup>2</sup> A scheme of the deposition chamber with dimensions is shown in Scheme S1.

More detailed information on the CVD set up and the CVD process can be found in our previous publications.<sup>1,3</sup>

As a next step, the Spiro-OMeTAD hole transport layer (HTL) was spin coated on top of the different (PPX-coated) perovskite thin films at 4000 rpm for 30 s. The Spiro-OMeTAD precursor solution was prepared by dissolving 79.8 mg Spiro-MeOTAD (Luminescence Technology) in 1 mL chlorobenzene (CB, Sigma-Aldrich) with the additives 17.5  $\mu\text{L}$  lithium bis(trifluoromethanesulfonyl) imide (Li-TFSI, Sigma-Aldrich) stock solution and 28.5  $\mu\text{L}$  4-tert-butylpyridine (TBP, Sigma-Aldrich). For oxygen doping, the samples were kept overnight in a dry box for 12 h and finally a 60 nm gold electrode was deposited by thermal evaporation through a shadow mask to define the active area to 0.105  $\text{cm}^2$ .

**Solar cells characterizations:** The solar cells were characterized using 21 Channel LED Solar Simulator (Wavelabs Solar Metrology Systems) inside a nitrogen filled glove box with an AM1.5G spectrum (100  $\text{mW cm}^{-2}$ ) calibrated to a KG5 short pass-filtered silicon reference solar cell. The  $J-V$  characteristics were measured in both reverse and forward direction with a constant scan rate of circa 0.6  $\text{V s}^{-1}$  (Keithley 2400 source measurement unit). The MPP was tracked by using a perturb-and-observe method. It should be mentioned that a 0.078  $\text{cm}^2$  mask was used to keep the active area constant for all solar cells throughout the measurements. The temperature of the solar cells set to 25  $^\circ\text{C}$  by an actively controlled Peltier element during  $J-V$  analyses and MPP tracking.

**UV-Vis spectrophotometry:** The absorption spectra of the perovskite thin films and EQE spectra of the PSCs were measured with a Bentham PVE300 photovoltaic service characterization system by illuminating the solar cell with modulated monochromatic light.

**Steady state and time resolved photoluminescence measurements:** Steady state photoluminescence (PL) measurements were performed using a custom-made PL setup. A pulsed

laser of 532 nm with a repetition rate of 1 kHz and a pulse width of 0.8 ns was used for the excitation of the samples. Time-resolved photoluminescence (TRPL) measurements were carried out in gated-mode. All measurements were performed with a pump fluence of  $\sim 400$  nJ/cm<sup>2</sup>. The photoluminescence was captured using an ACTON spectrometer and a CCD camera PIMAX512 at room temperature. The measurements were carried out in air.

**X-Ray diffraction (XRD):** The crystallinity of the perovskite thin films was examined by an XRD (D2Phaser from Bruker) machine with Cu-K $\alpha$  radiation ( $\lambda = 1.5405$  Å) in Bragg–Brentano configuration using a LynxEye detector.

**Atomic force microscopy (AFM):** Atomic force microscopy (AFM) was performed on a Dimension Icon AFM (Bruker, Karlsruhe, Germany) in standard tapping mode in air. Cantilevers of type HQ/NSC15/AI BS (MikroMasch) were used with a nominal force constant of 40 N m<sup>-1</sup> and a resonance frequency of 325 kHz. The roughness values were calculated using NanoScope Analysis 1.9 on selected areas of grains and averaged on five independent measurements.

**Scanning electron microscopy (SEM):** The cross section images were obtained with an environmental scanning electron microscope (ESEM; FEI Philips XL30 FEG-ESEM, Philips, Amsterdam, The Netherlands). The instrument is equipped with a secondary electron detector and the scanning was conducted under high vacuum conditions in SEM mode (voltage of 10 kV).

**Contact angle measurement:** The water contact angle (WCA) was measured with an optical contact angle meter (DSA100, Kruss, Hamburg, Germany). The measurement was performed at ambient temperature using the sessile drop measuring method provided by the software DSA3 (Kruss, Hamburg, Germany) for 5  $\mu$ L water droplets. The WCA values were averaged from five independent measurements.

**X-ray photoelectron spectroscopy (XPS):** XPS measurements were performed using a K-Alpha+ XPS spectrometer (Thermo Fisher Scientific, East Grinstead, UK). The data acquisition and processing using the Thermo Avantage software is described elsewhere.<sup>4</sup> All substrates were analyzed with a microfocused, monochromated Al K $\alpha$  X-ray source (400  $\mu\text{m}$  spot size). The K-Alpha+ charge compensation system was employed during the analysis, using electrons of 8 eV energy and low-energy argon ions to prevent any localized charge build-up. The spectra were fitted with one or more Voigt profiles (BE uncertainty:  $\pm 0.2$  eV) and the Scofield sensitivity factors were applied for quantification.<sup>5</sup> All spectra were referenced to the C 1s peak (C–C, C–H) at 285.0 eV binding energy controlled by means of the well-known photoelectron peaks of metallic Cu, Ag, and Au, respectively.

**Time-of-flight secondary-ion mass spectrometry (ToF-SIMS):** The ToF-SIMS experiments were performed on a TOFSIMS 5 machine (IONTOF GmbH, Münster, Germany) at IFG, KIT. The spectrometer is equipped with a Bi cluster primary ion source and a reflectron type time-of-flight analyzer. The UHV base pressure was  $< 8 \times 10^{-9}$  mbar. For a high mass resolution, the Bi source was operated in “high current bunched” mode providing short Bi<sub>3</sub><sup>+</sup> primary ion pulses at 25 keV energy, a lateral resolution of approx. 4  $\mu\text{m}$ , and a target current of 0.18 pA at 5 kHz. The short pulse length of 1 ns allowed for high mass resolution. Charge compensation was achieved using a low energy electron flood gun and suitable reflectron tuning. Spectra were calibrated on the omnipresent C<sup>-</sup>, C<sub>2</sub><sup>-</sup>, C<sub>3</sub><sup>-</sup>, or on the C<sup>+</sup>, CH<sup>+</sup>, CH<sub>2</sub><sup>+</sup>, and CH<sub>3</sub><sup>+</sup> peaks. Based on these datasets, the chemical assignments for characteristic fragments were determined. For depth profiling, a dual beam analysis was performed in a fully interlaced mode: The primary ion source was scanned on an area of 250 $\times$ 250  $\mu\text{m}^2$  (128 $\times$ 128 data points) and an argon cluster sputter gun (operated with Ar<sub>1200</sub><sup>+</sup> ions, 2.5 keV, scanned over a concentric field of 500 $\times$ 500  $\mu\text{m}^2$ , target current 0.75 nA) was

applied to erode the samples. The sputter ion dose density was  $> 1000$  times higher than the Bi ion dose density. In Fig. 1d, the sputter ion fluence was used as a measure for the erosion depth.

For Figure. S3, depth integrated  $C_8H_8^+$  signals were used. It should be noted, however, that this is not a standard approach for quantification of layered samples but rather an “experimental” metrology for dual beam depth profiling. Unlike in single beam depth profiling, some experimental conditions must be met. This approach is helpful for comparing the deposited amount of Ag in solar cells [6], but it also might become an interesting option for ultra-thin layers as in the presented study. The common approach to analyze layered systems and to quantify layer thicknesses with dual beam depth profiling in SIMS, uses the sputter time -more precisely the fluence of the sputter ions [ $1/\text{cm}^2$ ], based on beam current, scanned field of view and erosion time- to identify interfaces in the material stack and relating those regions of changing chemistry via the fluence to a depth scale via a calibrated sputter yield. Other than finding the interface(s) the absolute signal intensities are not needed. Keeping the sputter ratio of both beams (sputter beam fluence / analysis beam fluence) high, it is ensured that the analysis beam -often  $Bi_1^+$  or  $Bi_3^+$  at 20-30 keV- is not contributing significantly to the erosion and beam damage and mixing effects caused by the small, high energetic projectiles is minimized. Using this approach depth resolutions of a few nanometers have been reported. In very thin layers, however, problems arise due to not establishing an erosion/damaging equilibrium even if Ar cluster bombardment with lowest practical beam energies (here: 2.5 keV on a  $Ar_{1200}^+$  ion) is used. The attempt to quantify polymer layers being very thin, like in the present system, requires a different approach, that needs to be carefully evaluated on more systems. It is assumed that the depth integrated signal of a polymer specific fragment, like  $C_8H_8^+$  in this case, should be proportional to the deposited amount of polymer, even if the probing limit of a quasi-static experiment is exceeded by the polymer thickness (see Fig. S3). The most

important prerequisite of this metrology is keeping the sputter ratio of both beams constant by keeping their beam currents and scanned areas constant for all experiments. As stated earlier, in a conventional dual beam depth profile rising and falling flanks of characteristic signals are used to detect an interface, for further quantification only the applied fluence is used. This allows to change the beam current of the sputter gun (not the sputter ion energy!), or even use non-interlaced runs allowing any sputter ratio to be obtained, according to the depth that has to be reached in the current specimen. In the presented approach this is not feasible since a higher erosion beam current would inevitably reduce the absolute count rates obtained from the analysis beam. This creates a practical constrain for this kind of analysis: Comparing very different layer thicknesses is hindered since it can't be simply balanced by varying the sputter beam current in order to achieve suitable erosion times. So, in practice, studying a range of thicknesses from 0.2 nm to 5 nm would either require very long erosion times for the thick layers or introduce a reduced accuracy for the thinnest layers.

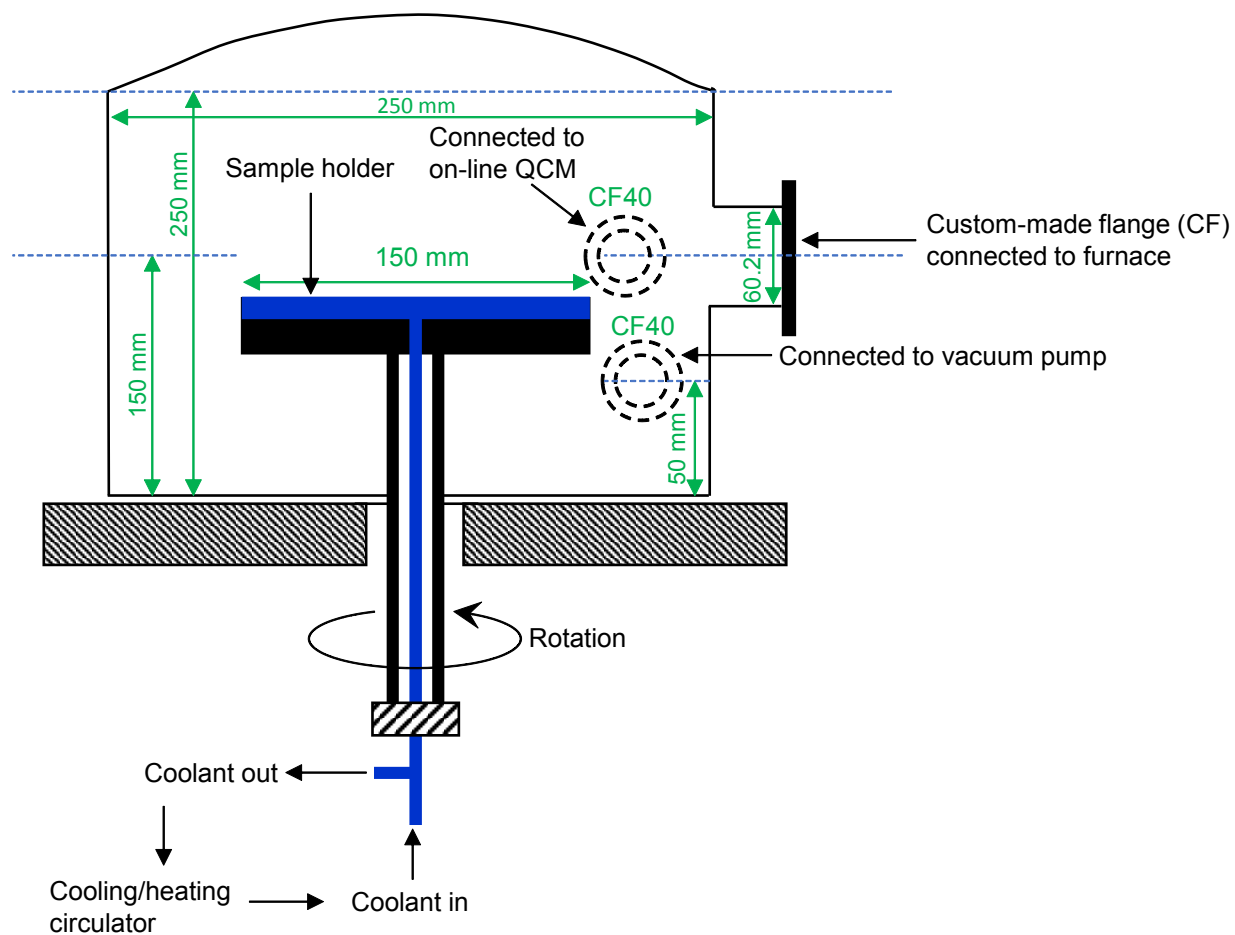
**Ellipsometry:** The thickness of the PPX layer was measured using spectroscopic ellipsometry in dry state (M44, Woollam Co., Inc., Lincoln NE, USA). The ellipsometry measurements were performed at an angle of incidence of  $65^\circ$  in the spectral region of 370–900 nm. The data were analysed by the CompleteEASE software (J.A. Woollam). The thickness measurements were recorded by fitting the ellipsometric  $\psi$  and  $\delta$  parameters with the An value of 1.65, and the Bn value of 0.01 for the PPX polymer layer using a Cauchy model in the software framework integrated with the system. The homogeneity of the coating was confirmed by analysing the results obtained from three independent experiments as shown in table S1.

**$V_{OC}$  vs. light intensity measurement:** For the extraction of ideality factor values, light intensity vs.  $V_{oc}$  measurements were performed on Paios (Fluxim AG) platform for all-in-one-

characterization of solar cells and light emitting diodes. A white-light LED (Cree XP-G) was used for the illumination.

**Stability test:** PSCs were kept in ambient atmosphere (relative humidity ~40-50%) under dark condition. The PSCs were periodically measured every three days.

## Supplementary Figures and Tables



**Scheme S1.** Simplified schematic of the deposition chamber of the CVD set up with dimensions.

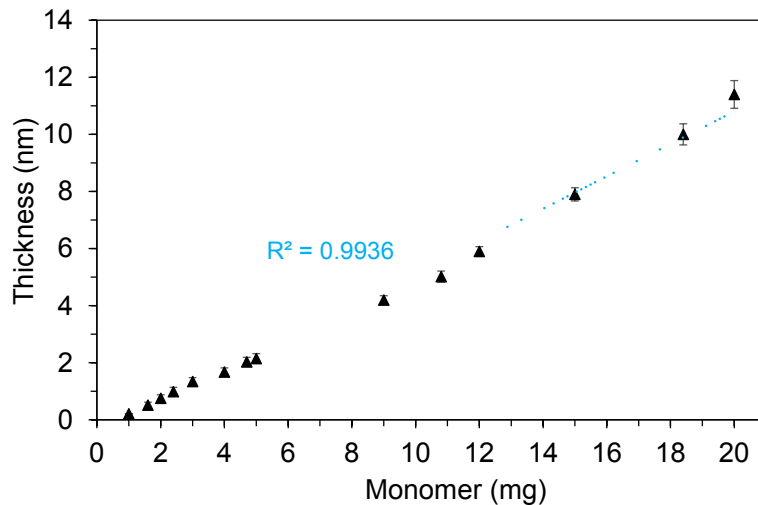


**Figure S1.** Deposition characteristic of PPX: thickness of the PPX layer as a function of the amount of the monomer fed into the CVD setup. A precise amount of the monomer was placed into a container from a stock solution of the monomer (20 mg/mL [2.2]paracyclophane in acetone). After evaporation of the solvent (<1 min), the container with monomer was transferred into the sublimation zone of the CVD and used to coat silicon wafers placed on the sample holder. The thickness values (nm) of PPX layer on the silicon wafer were obtained by ellipsometry.

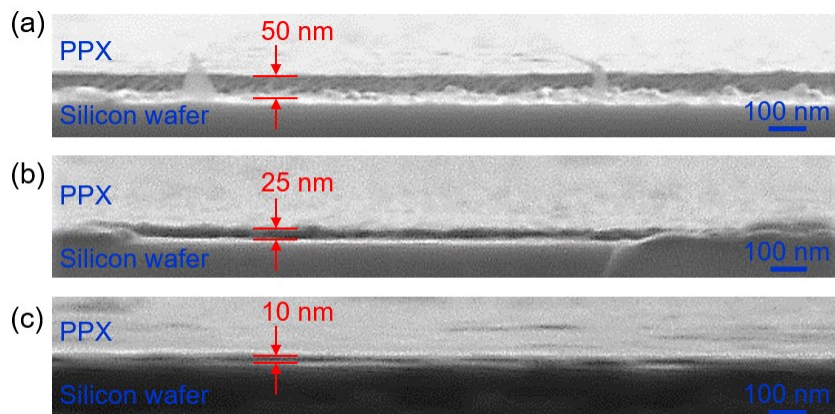


**Figure S2.** Deposition of a uniform and continuous film of PPX with controlled thickness: SEM images of the cross section of the silicon wafer coated with PPX layer with thicknesses of (a) 50 nm, (b) 25 nm, and (c) 10 nm.

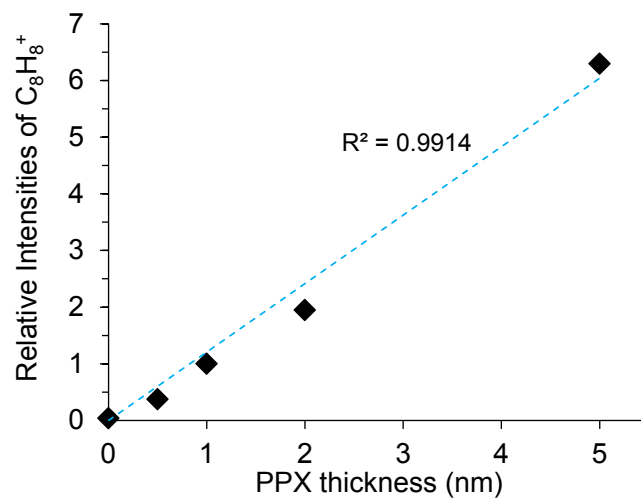


**Figure S3.** Relative intensity of depth integrated C<sub>8</sub>H<sub>8</sub><sup>+</sup> signals (characteristic for PPX polymer deposited on the surface of the perovskite) obtained from ToF-SIMS depth profiling of uncoated perovskite and perovskite coated with 0.5 nm, 1 nm, 2 nm, and 5 nm PPX.

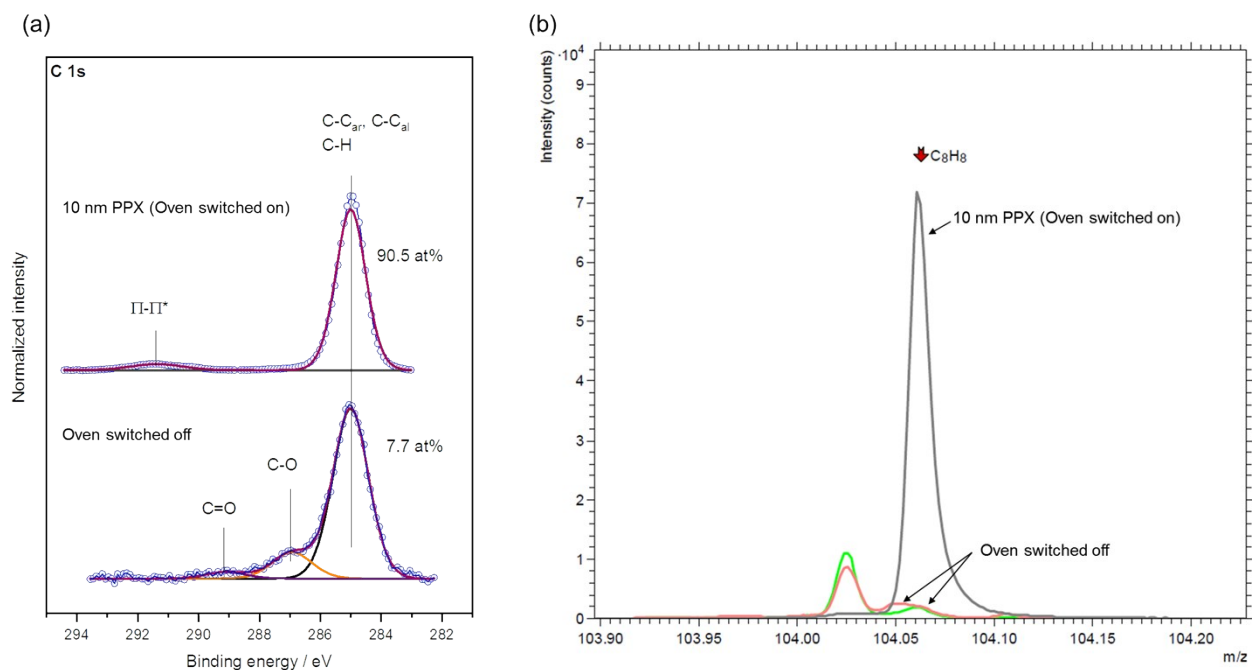


**Figure S4.** (a) Detailed XPS C 1s spectra of a silicon wafer placed on the sample holder of the CVD setup with switched off oven (no pyrolysis) (bottom) and of a silicon wafer coated with a 10 nm PPX layer obtained under normal CVD condition (oven switched on) after washing with ethanol and acetone (top). Only for the PPX layer, the weak  $\pi$ - $\pi^*$  transition signal at  $\sim 291.5$  eV is appearing. For a better visualization, all spectra are normalized to the maximum of intensity. (b) The C<sub>8</sub>H<sub>8</sub> fragment, although being present in the individual building blocks as well, is only detectable if the pyrolysis oven is used to create reactive species being able to form polymer (shown in gray color). Without pyrolysis no similar signal can be observed (shown in green and red color for sample before and after washing respectively).

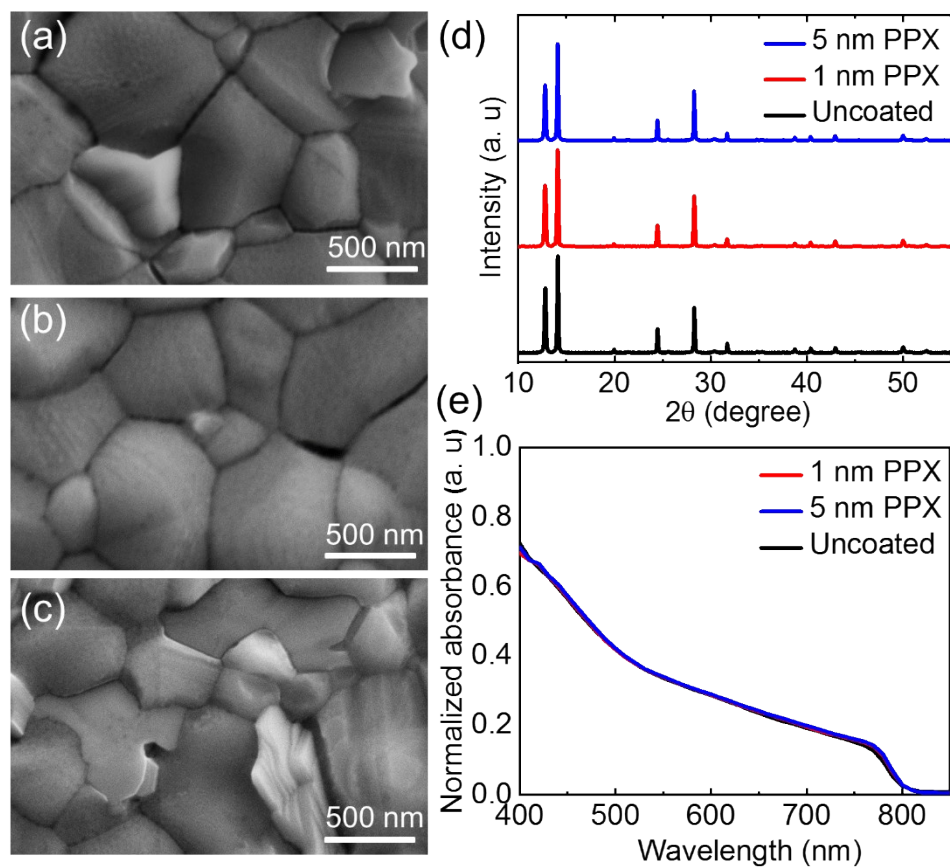


**Figure S5.** Top view SEM images of (a) uncoated, (b) 1 nm PPX-coated, and (c) 5 nm PPX-coated perovskite thin films. (d) XRD patterns and (e) normalized absorbance spectra the same samples.

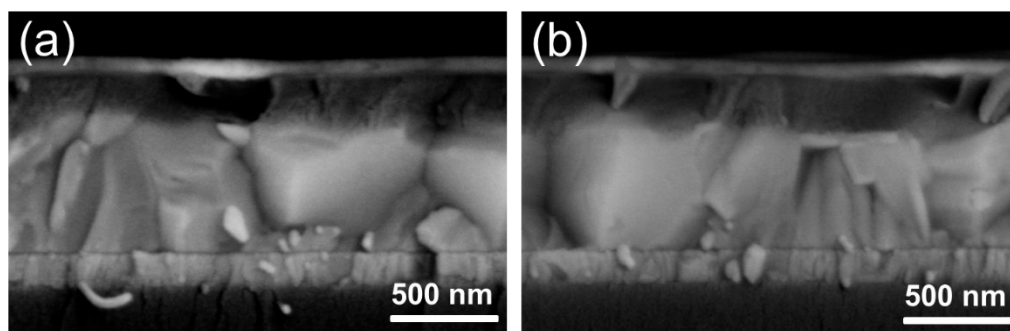


**Figure S6.** Cross-sectional SEM images of full PSCs fabricated by (a) uncoated and (b) 1 nm PPX-coated perovskite thin films.

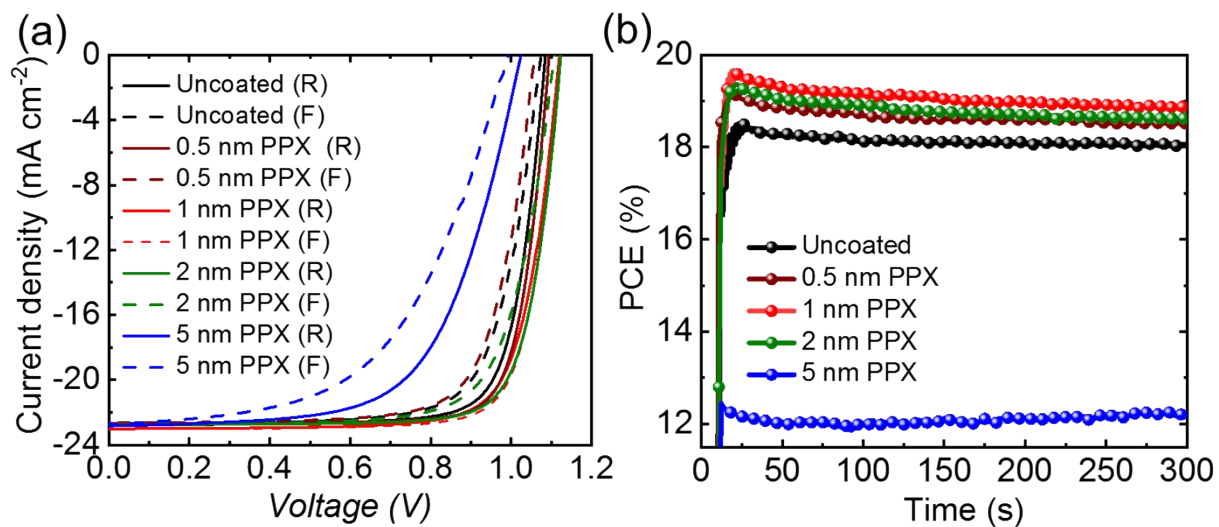


**Figure S7.** (a) Champion revers (R, solid line) and forward (F, dash line)  $J-V$  characteristics (b) stabilized PCEs during MPP tracking of PSCs fabricated with various thicknesses of the PPX passivation layer.

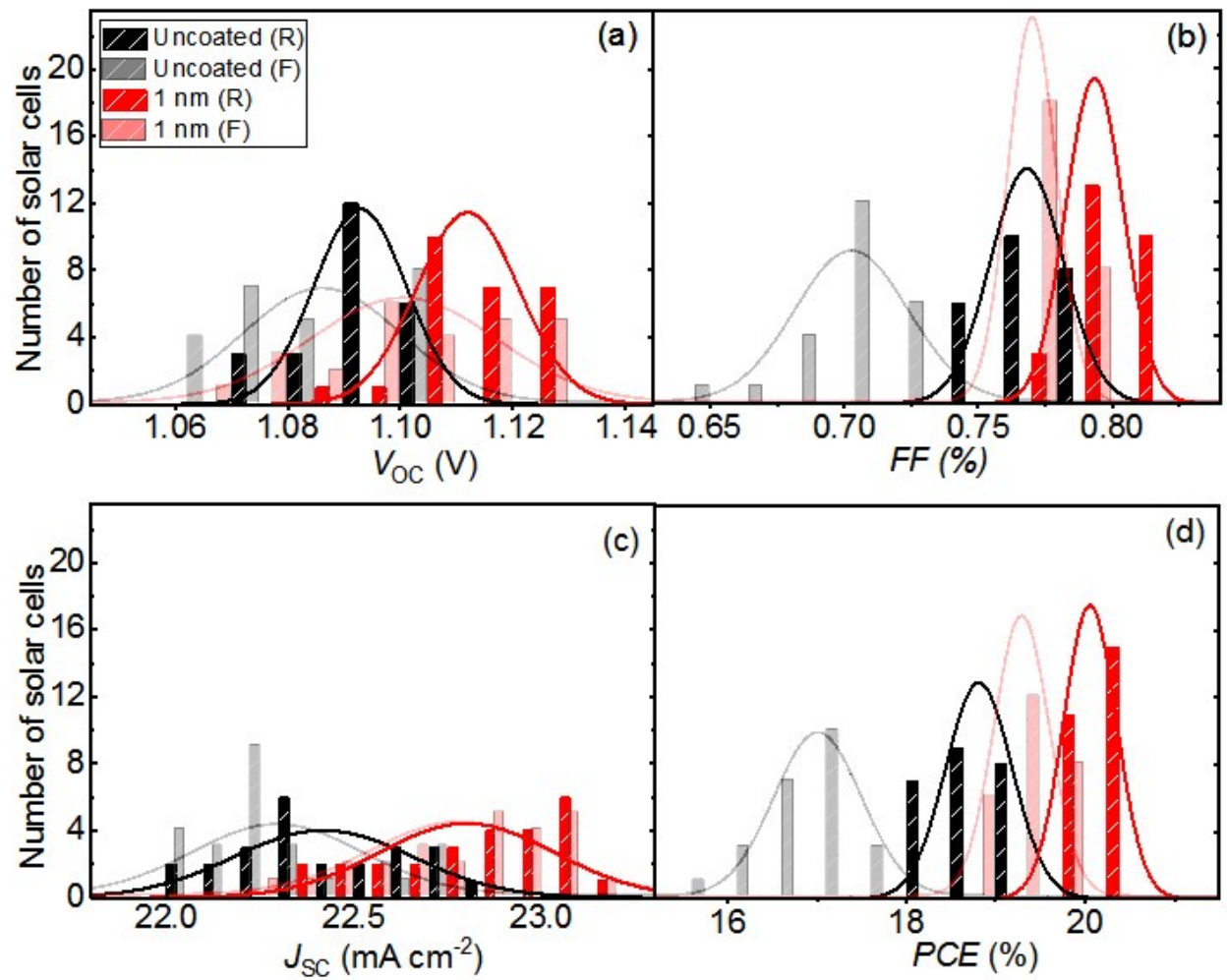
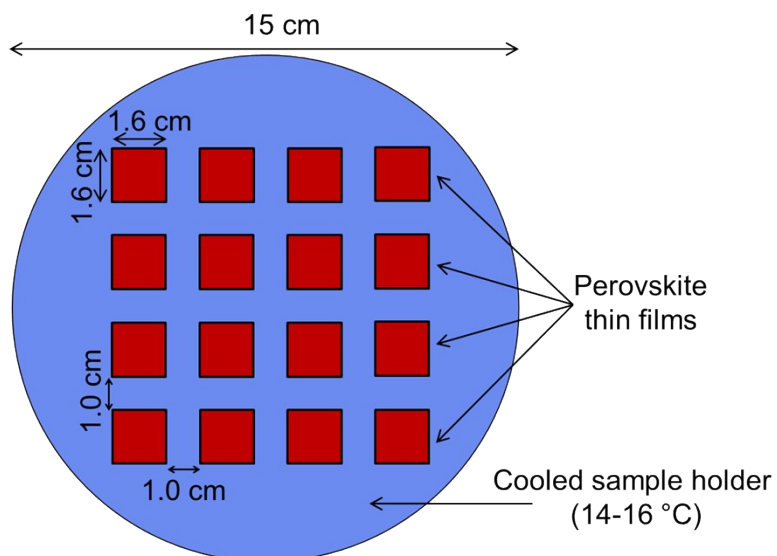


**Figure S8.** Histograms of the photovoltaic parameters in both revers and forward  $J$ - $V$  direction for 25 PSCs.



**Scheme S2.** Scheme showing the dimensions of the sample holder that enables to deposit PPX layer on a relatively large area of 15 cm in diameter. Up to 16 samples can be loaded on the sample holder in one run.

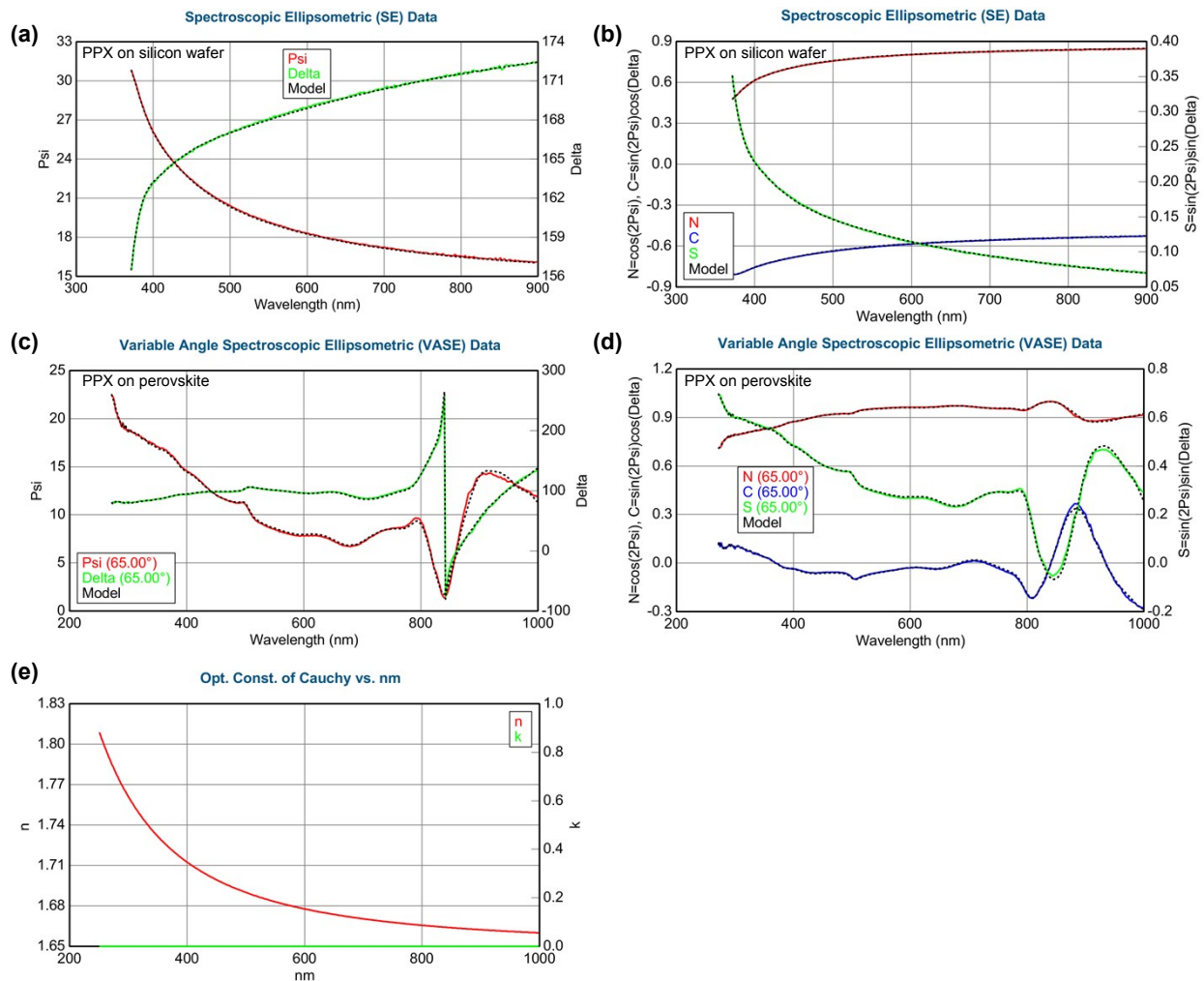


**Figure S9.** Measured data (Psi, Delta) from ellipsometry experiments (solid lines) of PPX layers of nominal thickness around 1 nm and the constructed model to describe the experimental data (dashed lines) using either (a,b) silicon wafer as the substrate or (c,d) perovskite as the substrate. (e) Optical constant refractive index ( $n$ ) of PPX layer (Cauchy model for transparent material assumes an extinction coefficient  $k = 0$ ) as a function of wavelength. Given that PPX exhibits some absorption for wavelength  $< 370$  nm, the refractive index is shown only for a limited spectral range (370 nm-900 nm). A mean squared error (MSE) of 1.302 (for silicon wafer sample) and 6.444 (for perovskite sample) with a thickness of  $1.02 \pm 0.072$  nm and  $1.05 \pm 0.141$  nm was obtained as a result of the fit for the PPX layer deposited on (a,b) the silicon wafer and (c,d) perovskite, respectively.

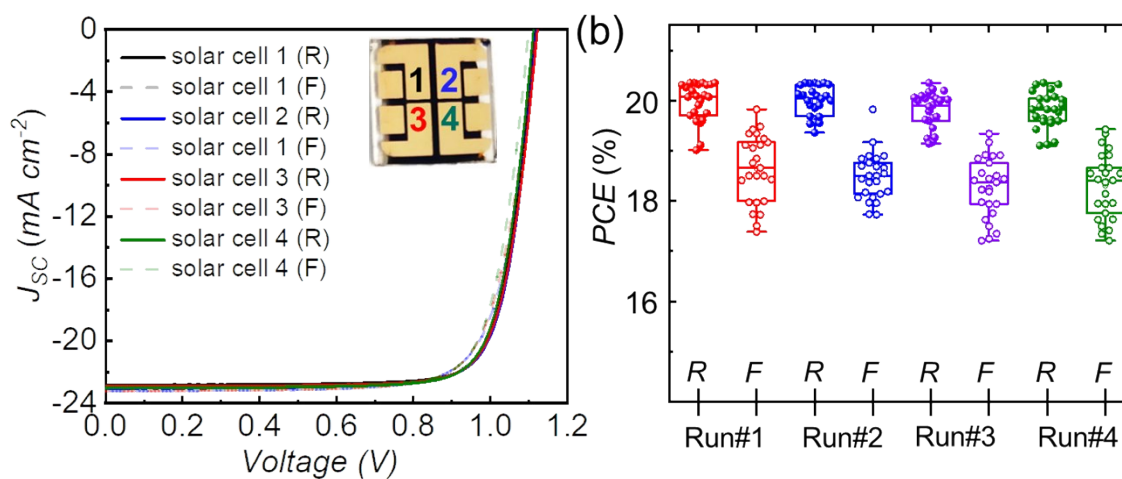


**Figure S10.** (a) Reverse (R) and forward (F)  $J$ - $V$  characteristics of four champion solar cells with 1 nm PPX-coated perovskite thin film (inset: photo of the device). (b) Power conversion efficiency (PCE) in both direction of 25 PSCs for different runs of CVD passivation.

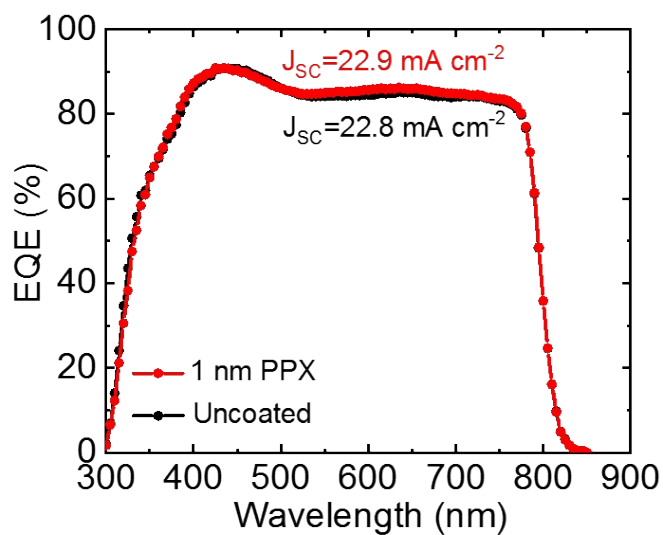


**Figure S11.** External quantum efficiency (EQE) spectra of PSCs incorporating an uncoated (black) and a 1 nm PPX-coated (red) perovskite thin film.

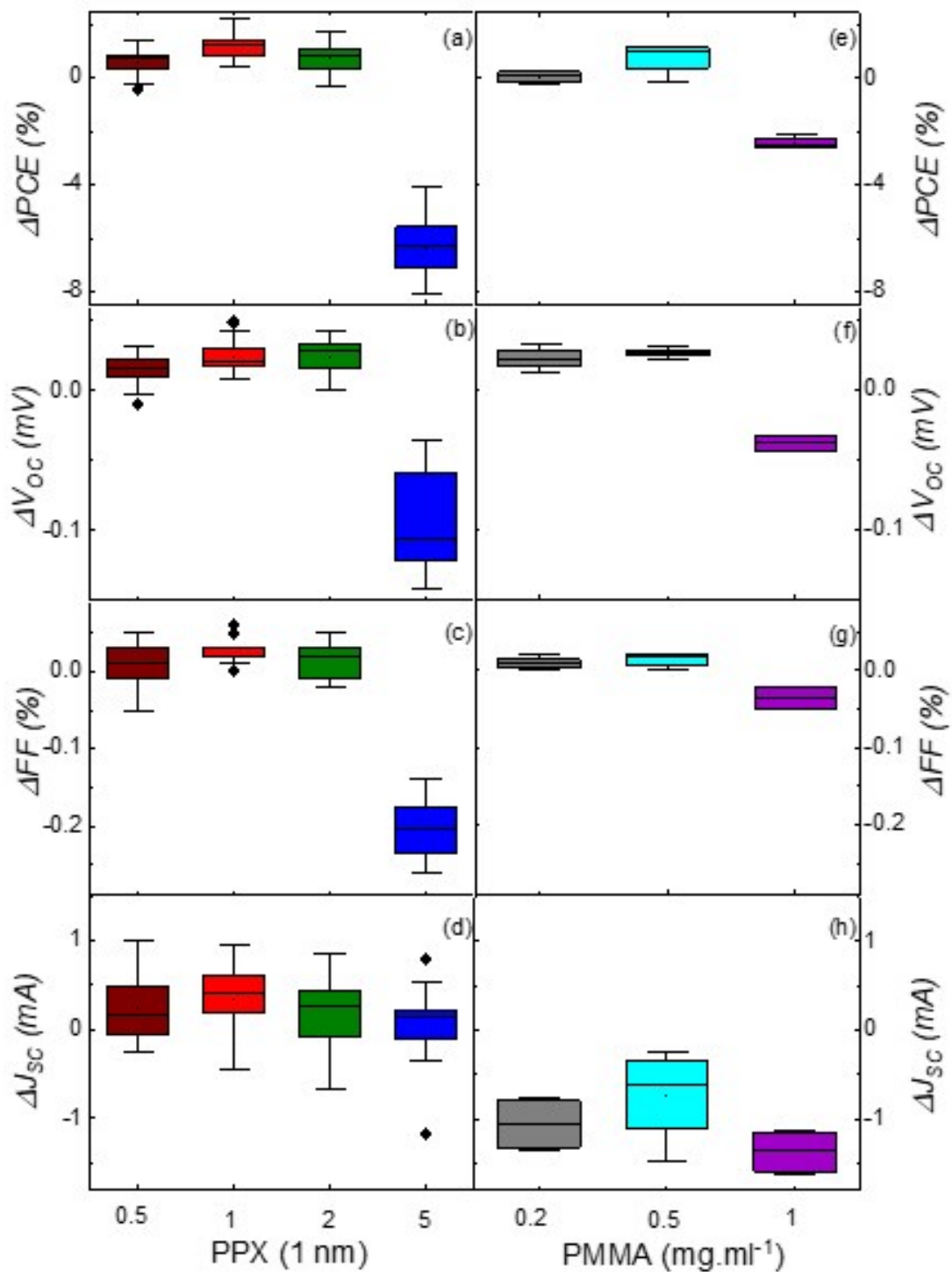


**Figure S12.** Delta ( $\Delta$ ) of photovoltaic parameters extracted from the  $J$ - $V$  measurement of different thicknesses of PPX passivation layers (a-c) and different concentration of PMMA solution that are used to spin coat the PMMA passivation (e-h).

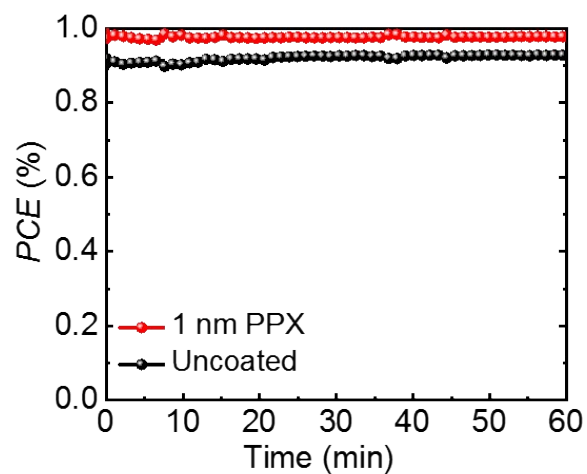


**Figure S13.** The normalized MPP tracking of the PSCs under continuous illumination for 60 min.

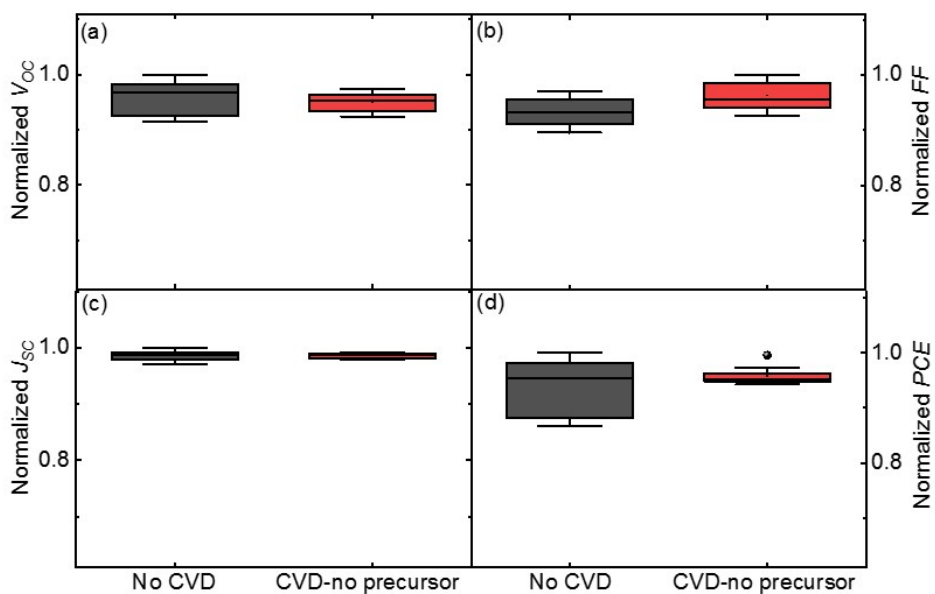


**Figure S14.** Photovoltaic parameters extracted from  $J$ - $V$  characteristics of 10 reference PSCs that were not exposed to a CVD process conditions (“No CVD”) and 10 PSCs that underwent the entire CVD deposition process but without any precursor being supplied during the deposition step: (a)  $V_{oc}$ , (b)  $FF$ , (c)  $J_{sc}$  and (d)  $PCE$ .

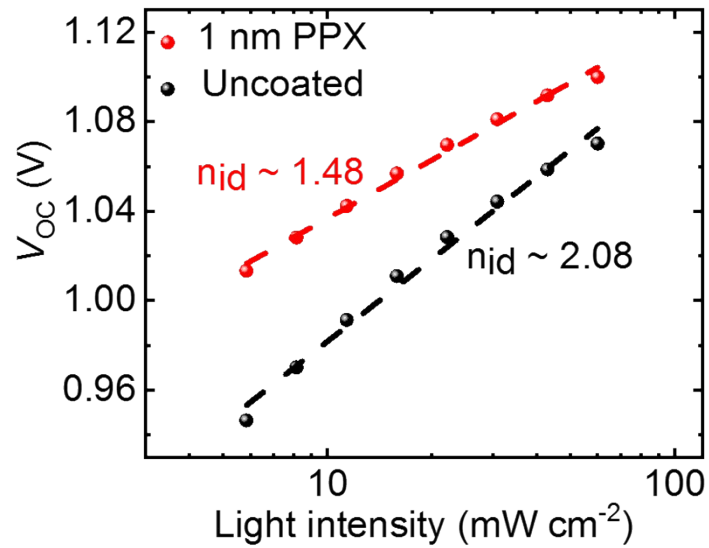


**Figure S15.**  $V_{OC}$  vs. light intensity measurements derived from PSCs incorporating an uncoated (black) and 1 nm PPX-coated (red) perovskite thin films.



**Figure S16.** Water contact angles (CA) measured on various perovskite thin films: (a) uncoated, (b) 1 nm PPX-coated and (c) 5 nm PPX-coated perovskite thin films.

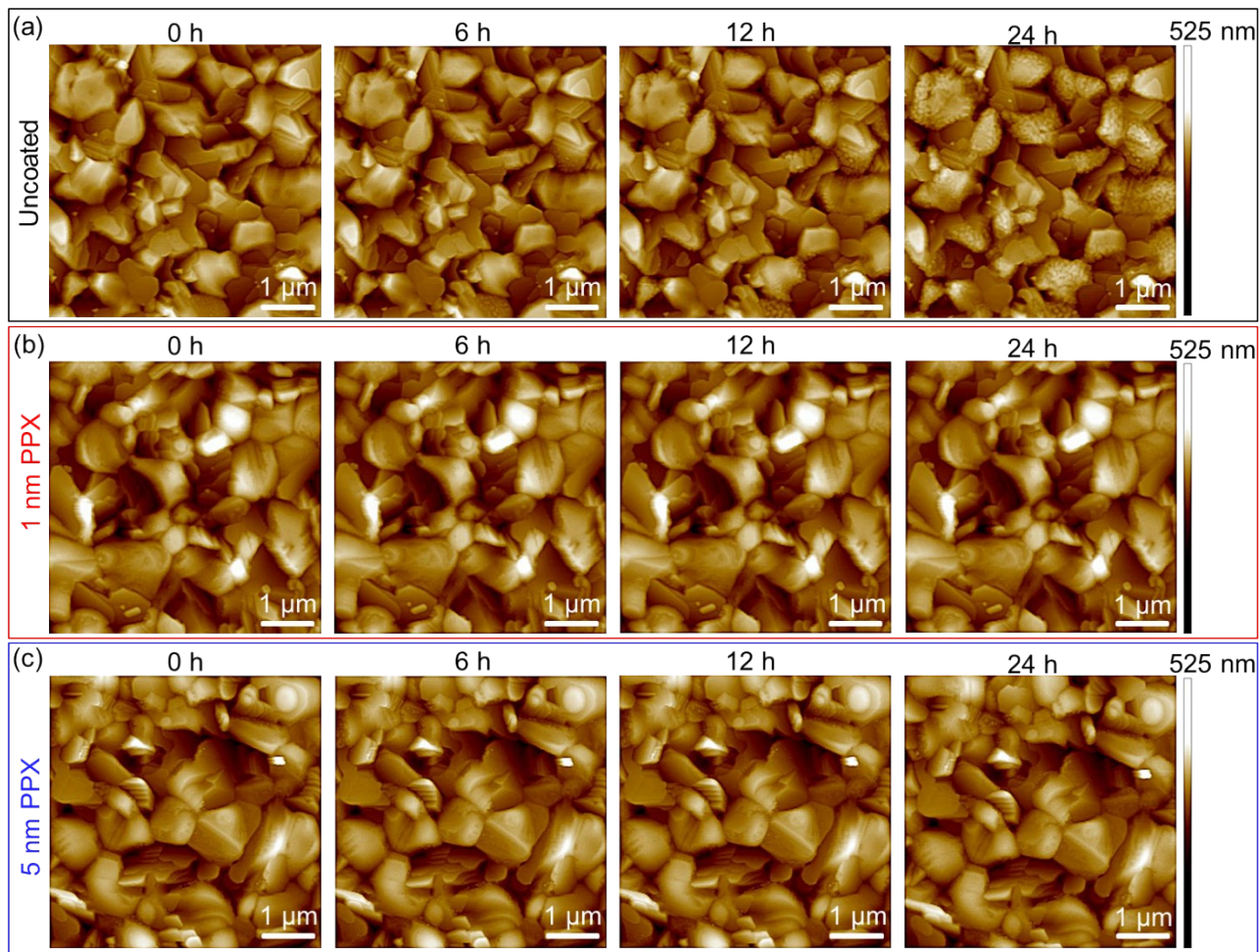


**Figure S17.** AFM images obtained at several time points from (a) uncoated, (b) 1 nm PPX-coated and (c) 5 nm PPX-coated perovskite thin films for 24 h under ambient air conditions.

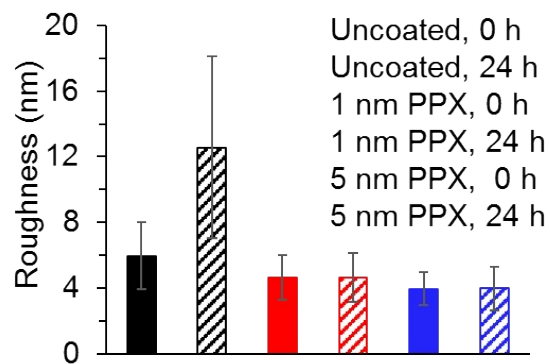


**Figure S18.** Surface roughness of marked perovskite grains for uncoated, 1 nm PPX-coated and 5 nm PPX-coated perovskite thin films before and after 24 h under ambient air conditions.

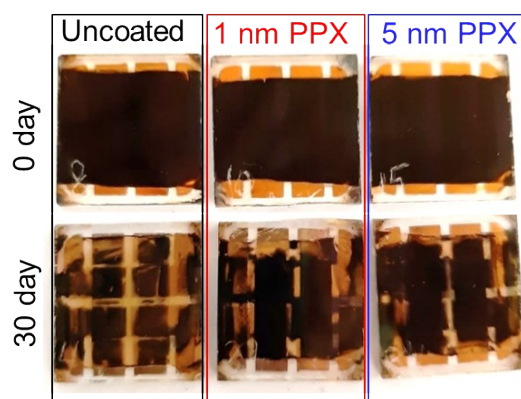


**Figure S19.** Photographs of PSCs fabricated by uncoated, 1 nm and 5 nm PPX-coated perovskite thin films at the beginning and after 30 days stability test.

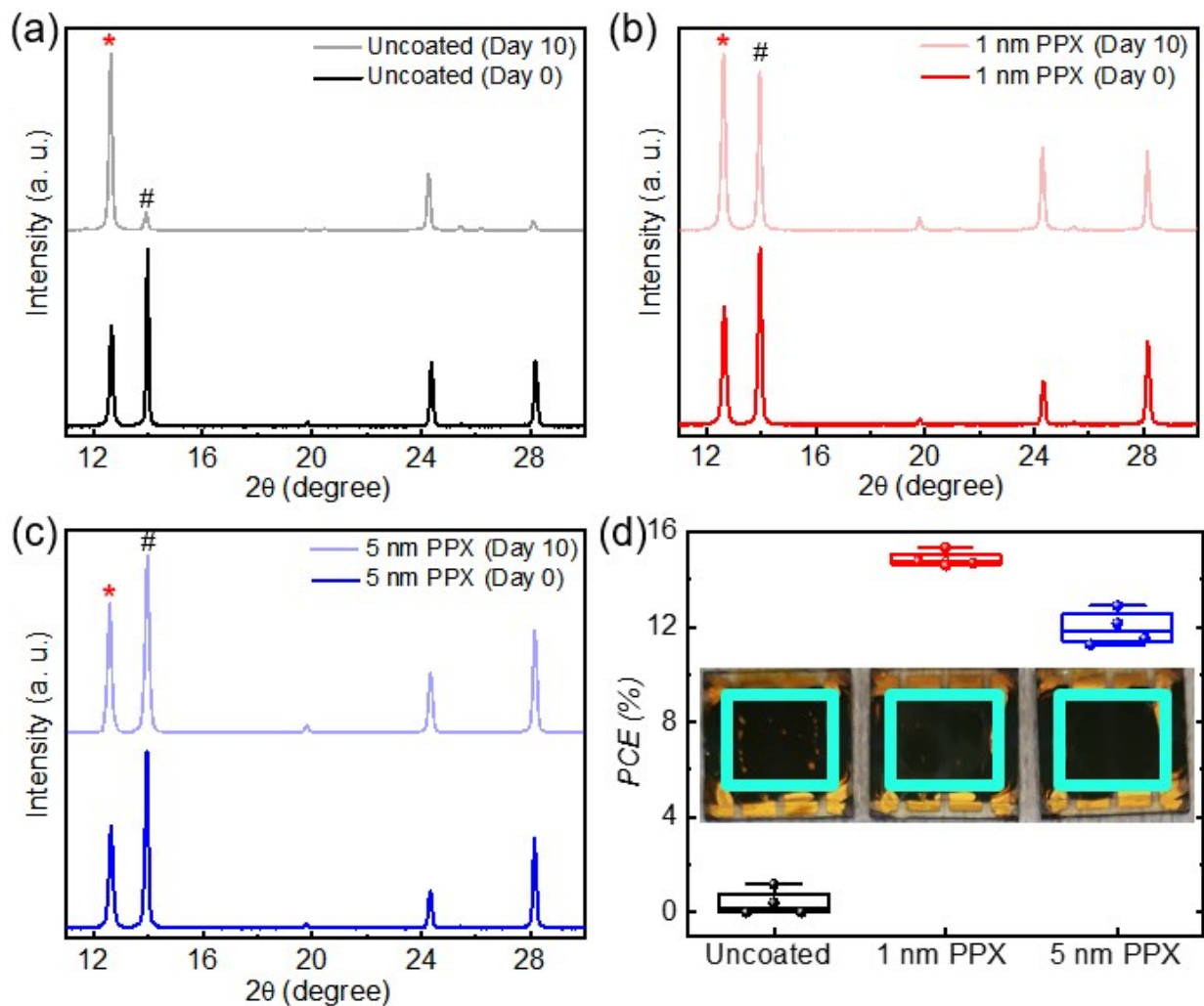


**Figure S20.** (a-c) XRD pattern of perovskite thin films without and with 1 nm and 5 nm PPX passivation layer. The XRD pattern of the films are compared before and after a humidity stress test (75% humidity, dark, 25 °C). (d) The PCEs and photographs (inset) of PSCs processed from perovskite thin films stressed as discussed in (a-c).

**Table S1.** Thickness values of PPX layer deposited on the perovskite surface determined by ellipsometry measurements, for several spots on three random substrates per PPX deposition (targeted thickness of 0.5 nm, 1 nm, 2 nm and 5 nm).

Sample name	Measurements	Thickness (nm)	Standard deviation
PPX-0.5 nm	Film 1	0.53	0.12
		0.4	
		0.69	
	Film 2	0.32	
		0.44	
		0.52	
	Film 3	0.63	
		0.51	
		0.67	
Average	0.52	0.12	
PPX-1 nm	Film 1	1.2	0.14
		1.05	
		0.89	
	Film 2	1.08	
		0.81	
		0.94	
	Film 3	1.17	
		0.84	
		0.96	
Average	0.99	0.14	
PPX-2 nm	Film 1	2.15	0.17
		1.91	
		2.06	
	Film 2	1.96	
		2.17	
		2.28	
	Film 3	1.94	
		2.09	
		1.72	
Average	2.03	0.17	
PPX-5 nm	Film 1	5.17	0.17
		4.71	
		5.05	
	Film 2	5.28	
		5.01	
		5.11	
	Film 3	5.1	
		4.82	
		4.97	
Average	5.02	0.17	

**Table S2.** Reverse (R) and forward (F) photovoltaic parameters of champion PSCs with various thicknesses of PPX layer.

PSC	<i>PCE</i> (%)	<i>FF</i> (%)	<i>V<sub>OC</sub></i> (V)	<i>J<sub>SC</sub></i> (mA cm <sup>2</sup> )	<i>R<sub>S</sub></i> ( $\Omega$ )
Uncoated (R)	19.4	78.5	1.08	22.8	31.2
Uncoated (F)	18.1	74.0	1.07	22.8	31.8
0.5 nm PPX (R)	20.0	80.5	1.09	22.7	30.2
0.5 nm PPX (F)	17.9	74.4	1.06	22.7	31.2
1 nm PPX (R)	20.4	79.2	1.12	23.0	34.1
1 nm PPX (F)	19.9	77.2	1.12	23.0	34.2
2 nm PPX (R)	20.2	79.0	1.12	22.8	34.4
2 nm PPX (F)	18.6	73.8	1.10	22.8	34.9
5 nm PPX (R)	14.6	62.8	1.02	22.8	78.7
5 nm PPX (F)	13.0	54.4	0.99	22.8	98.7

**Table S3.** Reverse (R) and forward (F) photovoltaic parameters obtained for four solar cells of the champion PSC fabricated by 1 nm PPX-coated perovskite thin film.

Solar cell	<i>PCE</i> (%)	<i>FF</i> (%)	<i>V<sub>OC</sub></i> (V)	<i>J<sub>SC</sub></i> (mA cm <sup>-2</sup> )
1 (R)	20.4	79.9	1.12	22.9
1 (F)	20.0	77.2	1.12	23.0
2 (R)	20.4	79.2	1.12	22.9
2 (F)	19.7	76.3	1.12	23.0
3 (R)	20.4	79.3	1.12	23.1
3 (F)	19.7	77.0	1.11	23.0
4 (R)	20.4	79.4	1.11	23.2
4 (F)	20.1	78.2	1.10	23.2

**Table S4.** Photovoltaic parameters obtained from the champion PSCs – under reverse (R) and forward (F) scans – fabricated by uncoated and 1 nm PPX-coated perovskite thin films.

PSC	<i>PCE</i> (%)	<i>FF</i> (%)	<i>V<sub>OC</sub></i> (V)	<i>J<sub>SC</sub></i> (mA cm <sup>-2</sup> )
Uncoated (R)	19.4	78.5	1.08	22.8
Uncoated (F)	18.1	74.0	1.07	22.8
1 nm PPX (R)	20.4	79.2	1.12	23.0
1 nm PPX (F)	19.9	77.2	1.12	23.0

## References

- [1] H.-Y. Chen and J. Lahann, *Langmuir*, **2011**, 27, 34–48.
- [2] J. Lahann, D. Klee, W. Pluester and H. Hoecker, *Biomaterials*, **2001**, 22, 817–826.
- [3] J. Lahann, *Polym. Int.*, **2006**, 55, 1361–1370.
- [4] K. L. Parry, A. G. Shard, R. D. Short, R. G. White, J. D. Whittle and A. Wright, *Surf. Interface Anal.*, **2006**, 38, 1497–1504.
- [5] J. H. Scofield, *J. Electron Spectros. Relat. Phenomena*, **1976**, 8, 129–137.
- [6] L. P. Mwakyusa, L. Leist, M. Rinke, A. Welle, U. W. Paetzold, B. S. Richards, M. Hetterich, *Thin Solid Films*, **2020**, 709, 138223.